

Enhancing the reliability of TOPCon technology by laser-enhanced contact firing

Xinyuan Wu ^a, Xutao Wang ^a, Weiguang Yang ^{b,*}, Jianjun Nie ^b, Jing Yuan ^b, Muhammad Umair Khan ^a, Alison Ciesla ^a, Chandany Sen ^a, Zhencong Qiao ^b, Bram Hoex ^{a,**}

^a School of Photovoltaic and Renewable Energy Engineering, University of New South Wales, Sydney, Australia, 2052

^b Jolywood (Taizhou) Solar Technology Co., Ltd., Taizhou, Jiangsu, 225500, China

ARTICLE INFO

Keywords:
TOPCon solar cells
Reliability
Damp-heat stability
Laser-assisted firing
Metallization
Glass-backsheet module

ABSTRACT

Tunneling oxide passivated contact (TOPCon) solar cells have made a considerable impact on the global photovoltaic (PV) market. Yet, its relatively poorer reliability compared to Passivated Emitter and Rear Contact (PERC) solar cells puts costly limitations on the module bill of materials that can be used. The use of silver/aluminum (Ag/Al) paste for front-side metallization is identified as a key factor contributing to the relatively poor reliability of TOPCon modules, particularly at high temperatures and humidity. However, very recently, laser-assisted firing techniques such as laser-enhanced contact optimization (LECO) that combine conventional co-firing at relatively low temperatures with a subsequent laser treatment have emerged as an appealing alternative to standard one-step cofiring. The main driver for laser-assisted firing is enabling higher power conversion efficiencies (*PCE*). This technique permits the application of screen printing pastes with considerably reduced levels of aluminum (Al), or even the complete exclusion of Al. Consequently, the enhancement in *PCE* values may not only boost *PCE*, but may also offer benefits in terms of reliability. This study investigates the impact of Jolywood Special Injected Metallization (JSIM) method on the reliability of TOPCon solar cells. Cell level damp heat testing at 85 °C and 85% relative humidity (DH85) with selected impurities reveals a significant improvement for the JSIM solar cells versus the standard baseline TOPCon cells. Baseline cells experienced rapid degradation, with a substantial (~92%_{rel}) loss in *PCE* attributed to a significant (~13,000%_{rel}) increase in series resistance (R_s) when exposed to sodium chloride (NaCl). Conversely, JSIM cells showcased remarkable resilience, displaying only a modest drop in *PCE* (~3.6%_{rel}) under similar conditions. This work clearly shows that laser-assisted firing processes such as JSIM also significantly improve the reliability of TOPCon solar cells. This improvement is due to the compatibility of these processes with screen printing pastes that have low or zero Al concentration for the TOPCon front. Consequently, this approach enables using more cost-effective materials for TOPCon modules, thereby reducing the overall cost of solar electricity.

1. Introduction

The advent of tunnelling oxide passivated contact (TOPCon) solar cells has garnered significant attention in pursuing high-efficiency silicon solar cell technologies over the past decade [1–5]. Recent strides in commercializing TOPCon cells, facilitated by diverse process and tool developments, position this technology as a potential frontrunner in the global photovoltaic market [6–13]. Despite its cost-effectiveness and compatibility with existing passivated emitter and rear contact (PERC) production lines, the widespread commercialization of TOPCon modules

has raised concerns regarding their reliability [14–19]. Numerous studies have highlighted potential reliability issues faced by TOPCon solar cells and modules under operational conditions, particularly under high humidity and temperature [14,15,20,21]. Damp-heat stress, exemplified by conditions such as the standard DH85 test (85 °C, 85% relative humidity), has been linked to substantial degradation in power output [18,22,23]. Investigations by Sommeling et al. and Iqbal et al. underscore the sensitivity of TOPCon cell front-side contacts to damp-heat conditions, culminating in severe contact issues after prolonged testing [14,15]. Previous research, including our own, has

* Corresponding author.

** Corresponding author.

E-mail addresses: yangwg01@jolywood.cn (W. Yang), b.hoex@unsw.edu.au (B. Hoex).

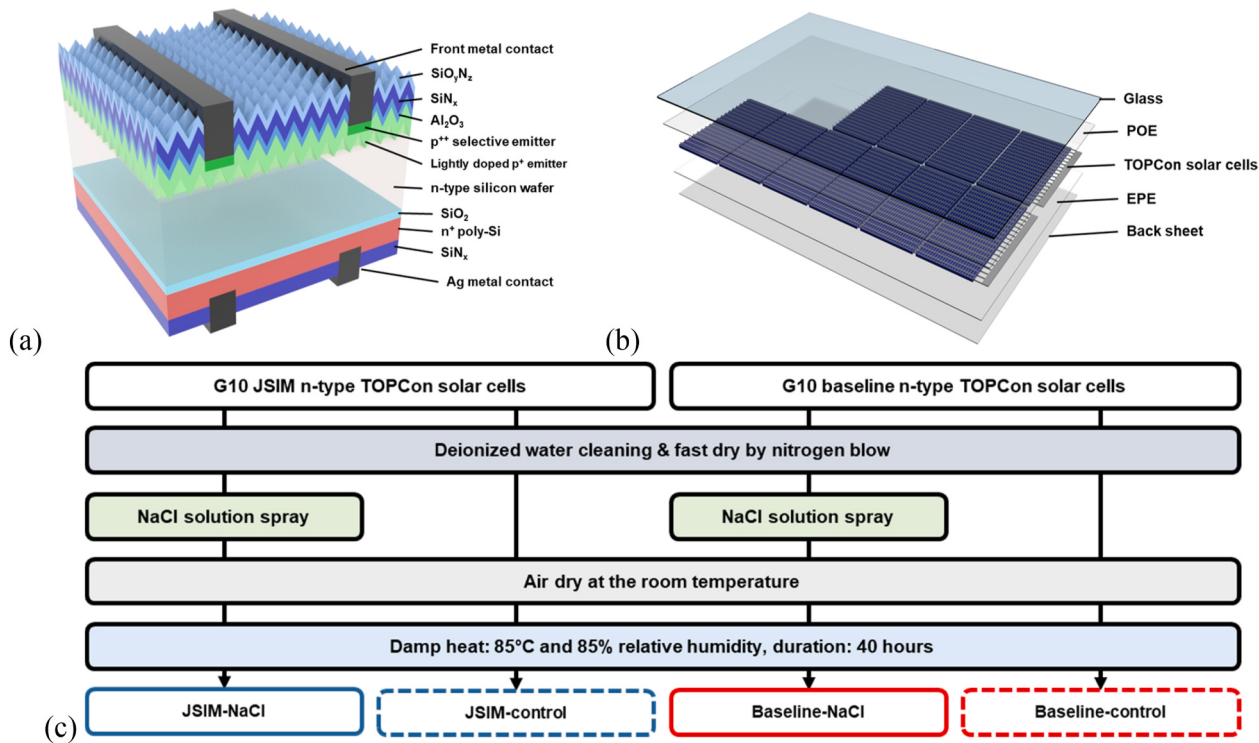


Fig. 1. (a) Schematic of the TOPCon solar cells and (b) the TOPCon modules used in this work. (c) The experimental flow of cell-level accelerated damp-heat testing.

demonstrated the heightened sensitivity of TOPCon front-side contacts to accelerated damp-heat testing, particularly when exposed to sodium chloride (NaCl), surpassing the susceptibility of PERC and silicon heterojunction (SHJ) solar cells [21]. Further exploration has implicated the relatively high Al content of the front contact as a critical factor contributing to the instability observed in TOPCon solar cells, warranting urgent optimization efforts [24–27]. Consequently, commercial TOPCon modules are primarily glass-glass (G-G) modules with high-quality encapsulants such as POE (polyolefin elastomers), and edge sealants to ensure that water cannot enter the module. However, this approach results in more expensive and heavier modules, so the industry is keen to address the intrinsic sensitivity of the TOPCon solar cells to allow for the use of cheaper module bill of materials.

In recent years, laser-assisted firing has garnered substantial interest as an improved firing technique for silicon solar cells [28–34]. Among these approaches, laser-enhanced contact optimization (LECO), which was initially introduced by Mayberry et al. entails applying a highly intense laser pulse locally on the front side of the solar cell under a constant reverse voltage [34]. This leads to a high localized current flow, which substantially reduces the contact resistivity between the semiconductor and metal electrode in areas where the contact resistance was already relatively low before the process [34–37]. This laser firing method has demonstrated efficacy in enhancing the efficiency of PERC and TOPCon cells by expanding the firing window and preserving surface passivation, particularly on lightly doped emitters. Furthermore, laser-assisted firing has facilitated the application of new metallization pastes for manufacturing PERC and TOPCon solar cells at lower firing temperatures, marking a significant advancement in industrial production lines utilizing TOPCon cells. The integration of laser-assisted firing has enabled the application of silver paste with low or zero aluminum on lightly doped boron emitters in TOPCon cells. Krassowski et al. investigated the reliability of PERC cells with LECO treatment, affirming that it did not compromise the long-term stability of module performance [36,38,39]. However, the evaluation of TOPCon cell and module reliability based on the laser-assisted firing process and tailored paste remains limited. Given the heightened sensitivity of TOPCon's front-side

contact, evaluating the impact of laser-assisted firing treatment and associated pastes on the long-term stability of TOPCon solar cells and modules, particularly under damp-heat conditions is imperative.

In this study, we employed contaminant-induced accelerated DH85 testing to assess industrial TOPCon solar cells using an optimized paste combined with the laser-assisted firing process, contrasting them with baseline TOPCon solar cells all fabricated at an industrial production line. The advantages of stability conferred by laser-assisted firing customized paste were revealed through detailed analysis of the contacts by scanning electron microscopy after accelerated testing. Additionally, glass-backsheet (G-B) modules were fabricated to conduct further long-term reliability testing of both baseline and laser-assisted firing-treated TOPCon solar cells.

2. Experimental details

All the TOPCon cells were processed on G10 n-type Czochralski (Cz) silicon wafers (182 mm × 182 mm). Fig. 1 (a) illustrates the structure of the TOPCon cell with selective emitters, while both experimental and control groups utilized TOPCon precursors where the TOPCon contact was made using plasma oxidation & plasma-assisted in situ-doping deposition (POPAID), a physical vapor deposition technique developed by Jolywood. The primary difference between the laser-treated and baseline samples was the front metallization process. The laser-treated group utilized Jolywood Special Injected Metallization (JSIM) in conjunction with customized Ag paste for the front contact formation on TOPCon solar cells. This involved a lower-temperature firing process to facilitate paste penetration through the front anti-reflection coating, culminating in the establishment of metal-semiconductor ohmic contact through whole-surface laser line scanning under reverse bias conditions. The laser operated at a wavelength of 1030 nm with a frequency of 1000 Hz. In contrast, the baseline samples underwent front metallization used standard commercial Ag/Al paste and a conventional firing process. Notably, both batches of TOPCon cells featured identical screen-printing pattern designs. Subsequent PV modules, comprising 144 half-cut cells, were produced via a standardized manufacturing process. Fig. 1 (b)

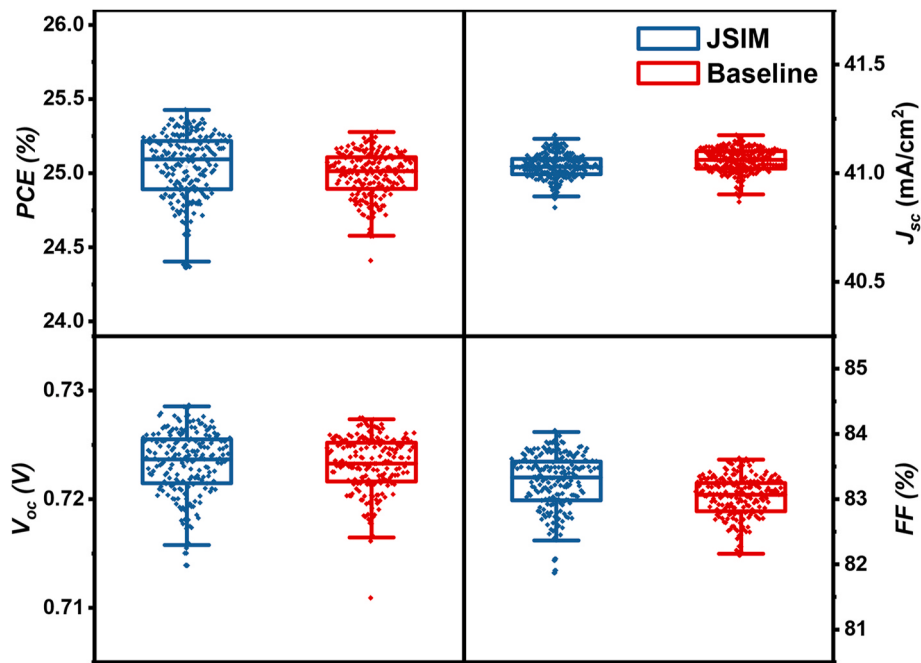


Fig. 2. Box plot of *I*-*V* related parameters of JSIM and baseline TOPCon solar cells from production lines.

portrays the schematic of the G-B module, with POE and expanded polyethylene (EPE) serving as the front and rear encapsulation materials, respectively.

Fig. 1 (c) shows the experimental flow of accelerated damp-heat testing. Prior to conducting the experimental procedures, the solar cells were cleaned using deionized water (DIW) followed by swift drying using a nitrogen gun to ensure all solar cells were clean before the experiment. Approximately 0.3 g of 0.9 wt% NaCl solution was delicately sprayed onto the front surface of selected samples, after which the samples were left to air dry naturally in a fume cupboard, maintaining room temperature and atmospheric conditions. Care was taken during the solution treatment phase to prevent contamination within and among the samples. After treatment, the samples were positioned vertically within individual polytetrafluoroethylene (PTFE) cassettes, spaced as such to mitigate cross-contamination during the damp-heat testing phase. The DH85 tests were done in an ASLi Environment chamber set to a temperature of 85 °C and a relative humidity of 85%. The chamber was cycled to room temperature between each measurement period (10 h) and reheated for subsequent stages of damp-heat treatment.

We used two systems to determine the current-voltage (*I*-*V*) characteristics of solar cells. A Halm inline measurement system with a calibrated reference cell was used at the industrial production line and a LOANA solar cell analysis system for accelerated DH85 testing. From the *I*-*V* measurements, we extracted the power conversion efficiency (PCE), short-circuit current density (J_{sc}), open-circuit voltage (V_{oc}), fill factor (FF), and series resistance (R_s). The module-level DH85 testing followed IEC TS 62782:2016, and the module's output was measured by a GIV-2000DS2616 flash tester from Gsolar Power [40]. Utilizing a BTImaging R3 tool equipped with a high open-circuit voltage lens, we generated photoluminescence (PL) and R_s images. Subsequent processing of luminescence images was carried out using LumiTools [41]. To evaluate the contact resistance, we specifically focused on the non-busbar regions of the TOPCon cells. Employing a FOBA M1000 scribing laser, we created 6 mm wide stripes for contact resistance assessment. The quantification of contact resistances involved utilizing the transfer length method (TLM) facilitated by a PV-tools TLM-SCAN+. Measurements were conducted before and after subjecting the cells to a 20-h accelerated DH85 test.

Table 1

The batch average *I*-*V* results of JSIM and baseline TOPCon solar cells.

Group	Number of Cells	PCE (%)	J_{sc} (mA/cm ²)	V_{oc} (mV)	FF (%)
JSIM	201	25.1 ± 0.2	41.0 ± 0.1	723.3 ± 0.3	83.2 ± 0.4
Baseline	198	25.0 ± 0.1	41.0 ± 0.1	723.2 ± 0.2	82.9 ± 0.3

Moreover, a Zeiss 550 Crossbeam cryo-focused ion-beam scanning electron microscope (cryo-FIB-SEM) was utilized to obtain cross-sectional images for analyzing metal contacts. Operating at 1.5 nA, the SEM probe maintained a high-tension electron (EHT) voltage of 20 kV. In standard kV mode, the FIB probe was configured to 30 kV and 50 pA. Under identical SEM conditions, energy dispersive spectroscopy (EDS) analysis using the Oxford Instruments Ultim® Max was performed, followed by result processing with AZtec software to reveal silver (Ag), lead (Pb), aluminium (Al), oxygen (O), sodium (Na) and chlorine (Cl).

3. Results and discussion

3.1. Cell performance

Fig. 2 and Table 1 show the *I*-*V* results of JSIM and baseline TOPCon solar cells. The average PCE for JSIM cells was 25.1%, slightly higher than the baseline cells at 25.0%. Notably, the short-circuit current density (J_{sc}) and open-circuit voltage (V_{oc}) of the baseline and JSIM TOPCon solar cells were quite similar. The primary divergence lay in the fill factor (FF), with JSIM having a FF of 83.2%, surpassing the baseline with a value of 82.9%. This underlines JSIM's ability to allow for higher quality contacts enabled by the Ag screen printing paste without Al and the wider firing process window. To ensure direct comparability under accelerated DH85 testing in our subsequent stage, cells with average efficiency were chosen.

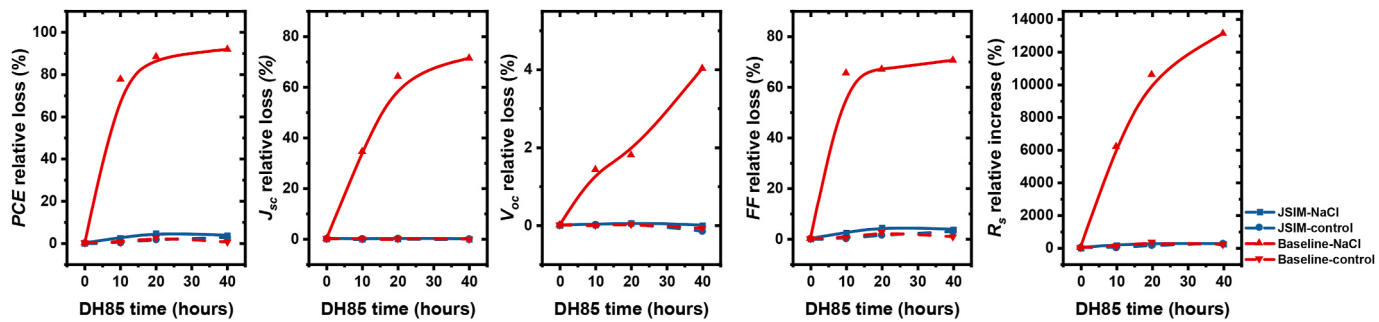


Fig. 3. Relative changes in PCE, J_{sc} , V_{oc} , FF and R_s as a function of DH85 time for JSIM and baseline TOPCon samples.

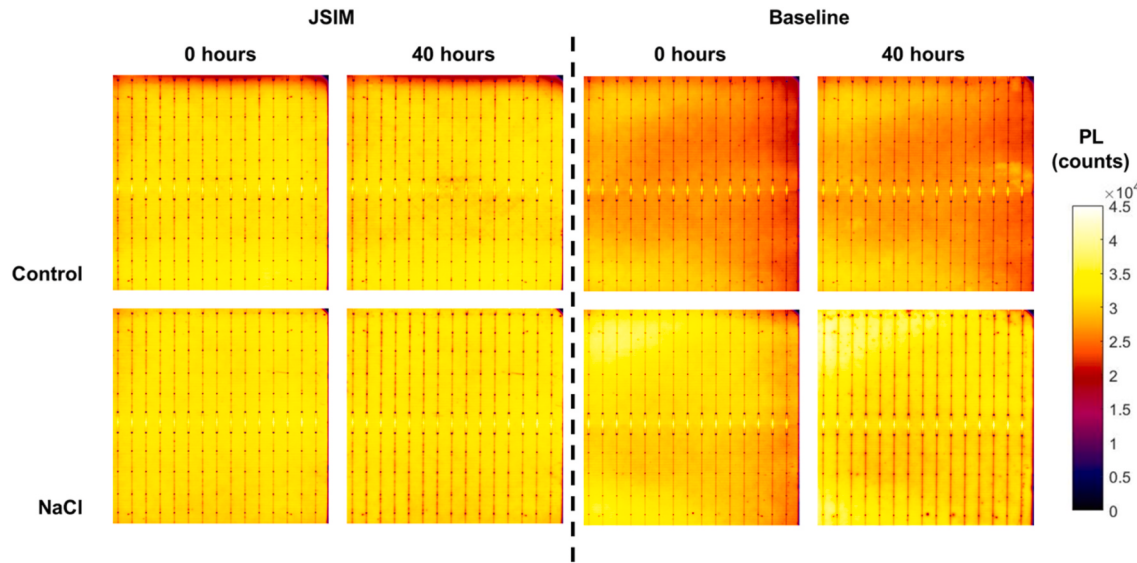


Fig. 4. PL images of TOPCon solar cells from each experimental group before (top) and after (bottom) 40-h DH85 testing.

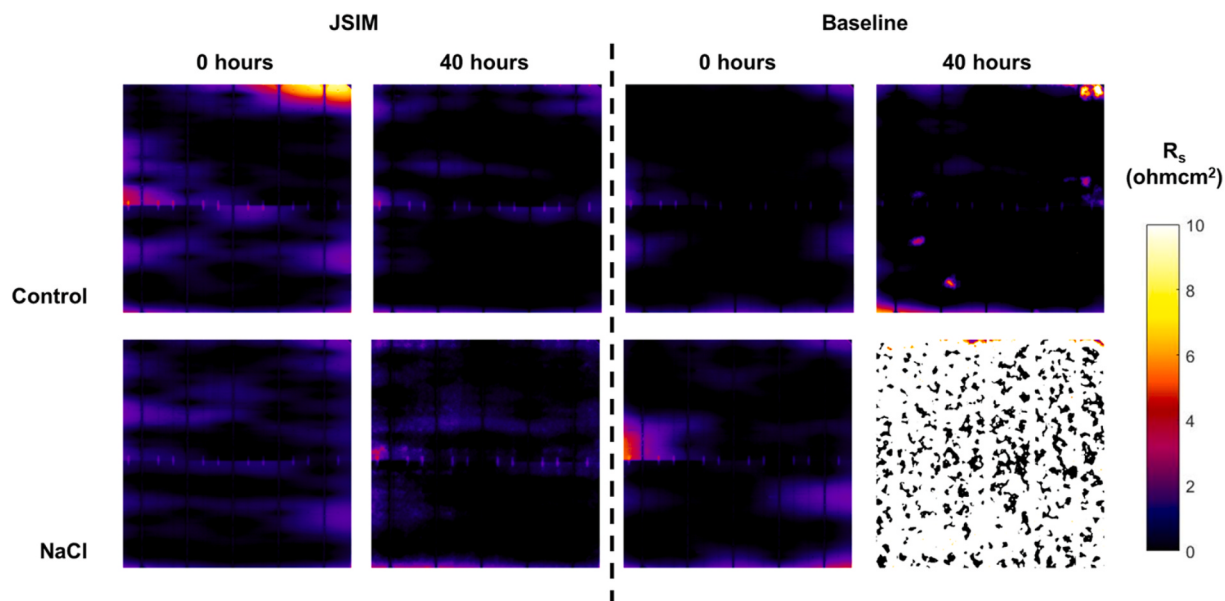


Fig. 5. R_s images of TOPCon solar cells from each experimental group before (top) and after (bottom) 40-h DH85 testing.

3.2. Cell-level accelerated DH85 test

The DH85 testing was conducted over a duration of 40 h, and the

variations in cell performance are shown in Fig. 3. Throughout the entire DH85 testing period, the control samples showed consistently stable performance. Conversely, consistent with our prior observations [21],

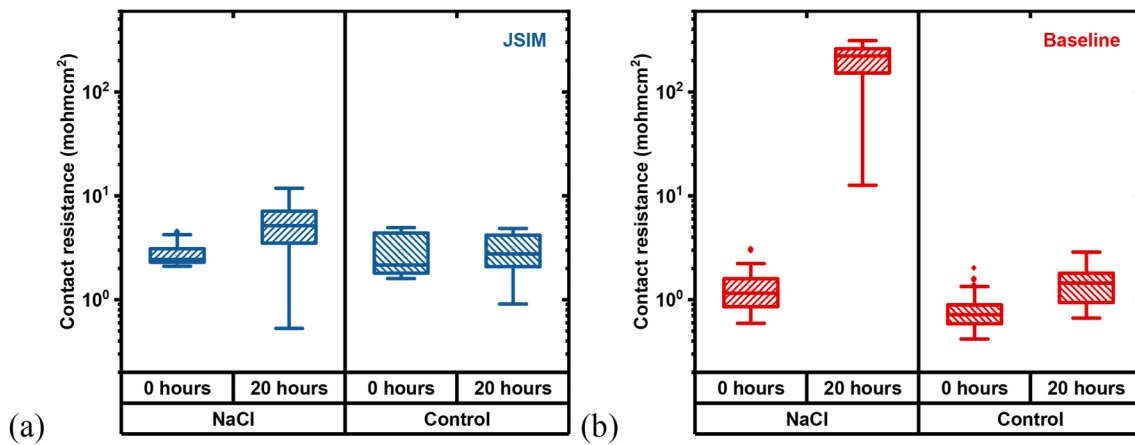


Fig. 6. The front-side contact resistance (ρ_c) of the NaCl-sprayed and control stripes from (a) JMIS and (b) baseline TOPCon solar cells before and after 20 h of DH85.

the baseline samples demonstrated rapid degradation, degrading by up to $\sim 92.0\%$ _{rel} after the 40-h DH85 test. Notably, the R_s of the Baseline-NaCl cells exhibited an approximately $\sim 13,000\%$ _{rel} increase after 40 h. This very high series resistance also affected the measured J_{sc} value as the current extraction of the solar cell was impeded by the higher resistive losses. In contrast, JSIM samples only showed a PCE degradation of approximately $\sim 3.6\%$ _{rel} after 40 h of DH85. The degradation in JSIM samples primarily stemmed from an increase in R_s of $\sim 240\%$ _{rel}, which was significantly lower than the baseline TOPCon solar cells.

The PL and R_s images of the JSIM and baseline solar cells are shown in Figs. 4 and 5. The PL images reveal no significant changes, indicating that the DH85 testing does not increase the overall recombination for the TOPCon solar cells in this study. However, some darker regions can be seen along the busbars of the samples. This suggests that the silicon-metal interface may be affected during the DH85 testing, leading to localized recombination issues in specific areas. In the Baseline-control group, an increase in R_s was observed for some regions, potentially due to accidental contamination or damage during the experiment. Notably, the R_s image of the Baseline-NaCl group shows a significant increase in R_s over the whole solar cell area after 40 h of DH85, consistent with the I-V changes shown in Fig. 3. The entire metal contacts on the surface were significantly affected by NaCl during DH85 testing. Conversely, the JSIM-NaCl samples did not show any significant degradation. While some regions displayed slight R_s increases, the majority of the surface maintained relatively low R_s levels. This indicates that the metal contacts in JSIM samples exhibited significantly less sensitivity to NaCl-induced deterioration, resulting in TOPCon solar cells that can withstand NaCl during DH85.

3.3. Contact resistance

To get more insight into the cause for the increased R_s , we investigated the contact resistances of JSIM and baseline samples both before and after 20 h of DH85 testing and the results are shown in Fig. 6. Across all control groups, there was a limited increase compared to the contaminated groups. In the JSIM-control group, the average measured contact resistance (ρ_c) was approximately $\sim 2.9 \text{ mOhm}\cdot\text{cm}^2$ before testing and slightly increased to $\sim 3.1 \text{ mOhm}\cdot\text{cm}^2$ after the 20 h of DH85. Similarly, the Baseline-control group exhibited no significant increase after DH85 testing, with values ranging from 0.8 to 1.5 $\text{mOhm}\cdot\text{cm}^2$. However, the ρ_c of Baseline-NaCl dramatically escalated from 1.3 to 200.6 $\text{mOhm}\cdot\text{cm}^2$ after 20 h of DH85. The slightly higher contact resistance for the JSIM group indicates that there is still room to further improve the contact formation using the JSIM process. For the JSIM-NaCl group, the initial ρ_c measured $\sim 2.7 \text{ mohm}\cdot\text{cm}^2$ increased to $\sim 5.6 \text{ mohm}\cdot\text{cm}^2$ after the 20 h of DH85, which is orders of magnitude better

compared to the baseline samples. This clearly shows that the baseline samples were more susceptible to corrosion, while JSIM samples exhibited a substantial higher tolerance against NaCl-induced damage. Consequently, laser enhanced firing processes such as JSIM may enable TOPCon solar cells with a materially improved corrosion reliability.

3.4. FIB-SEM cross-section images

To further investigate the contact failure mechanisms, we employed focused ion-beam techniques to acquire polished sections of the metal contacts. Alongside capturing SEM images, we utilized EDS for elemental analysis of the metal contacts. Fig. 7 (a) and (c) depict metal contacts predominantly composed of Ag which is as expected. The baseline samples clearly show the presence of Al in the contact, while no Al was detected in the JSIM metal contacts in this work. Notably, the edges of the Al-rich regions exhibited an overlay of O, indicating that the Al in the contact was partially oxidized. Additionally, no Na or Cl was detected in the EDS analysis of control samples.

Fig. 7 (b) shows the Baseline-NaCl sample after 20 h of DH85 which looks substantially different from the Baseline-control sample. The Baseline-control samples kept the Al round particle state after DH85 testing, but, for Baseline NaCl, the internal distribution of Al was no longer concentrated but dispersed within the contact. Additionally, traces of O and Cl overlapped with Al, suggesting that the Al was corroded and oxidized by NaCl. This aligns with findings in the literature on Al alloy corrosion [42–45]. Due to the difference in electronegativity, Al exhibits a higher reactivity compared to Ag, potentially leading to galvanic corrosion within Ag/Al fingers [46]. As a result, under conditions involving active anions such as chloride ions in the presence of water at elevated temperatures, Al readily undergoes oxidation. This results in the loss of Al metallic properties, thereby affecting the electrical characteristics of the metal contacts. Consequently, voids were formed in these regions, and the remaining Al reacted with either O or Cl, rendering it ineffective in the contact mechanism. Moreover, this corrosion was not limited to the interior of the metal contact but could also extend to the interface between the metal contacts and Si surfaces. Given that Al can form Ag/Al spikes during the contact firing step [47, 48], corrosion of Al might also alter the interface contact properties, leading to a significant increase in contact resistance as illustrated in Fig. 6 (b). Furthermore, the Pb in Baseline-NaCl exhibited overlap and influence from Cl, potentially a side effect of Al redox reactions. PbO plays a key role in the fritting process as well as in the quality of the contact between silicon and silver. These effects collectively contributed to the rapid and severe increase in R_s observed in Figs. 3 and 5.

Conversely, the JSIM contacts displayed significantly less deterioration by NaCl after 20 h of DH85, as depicted in Fig. 7 (d). We observed

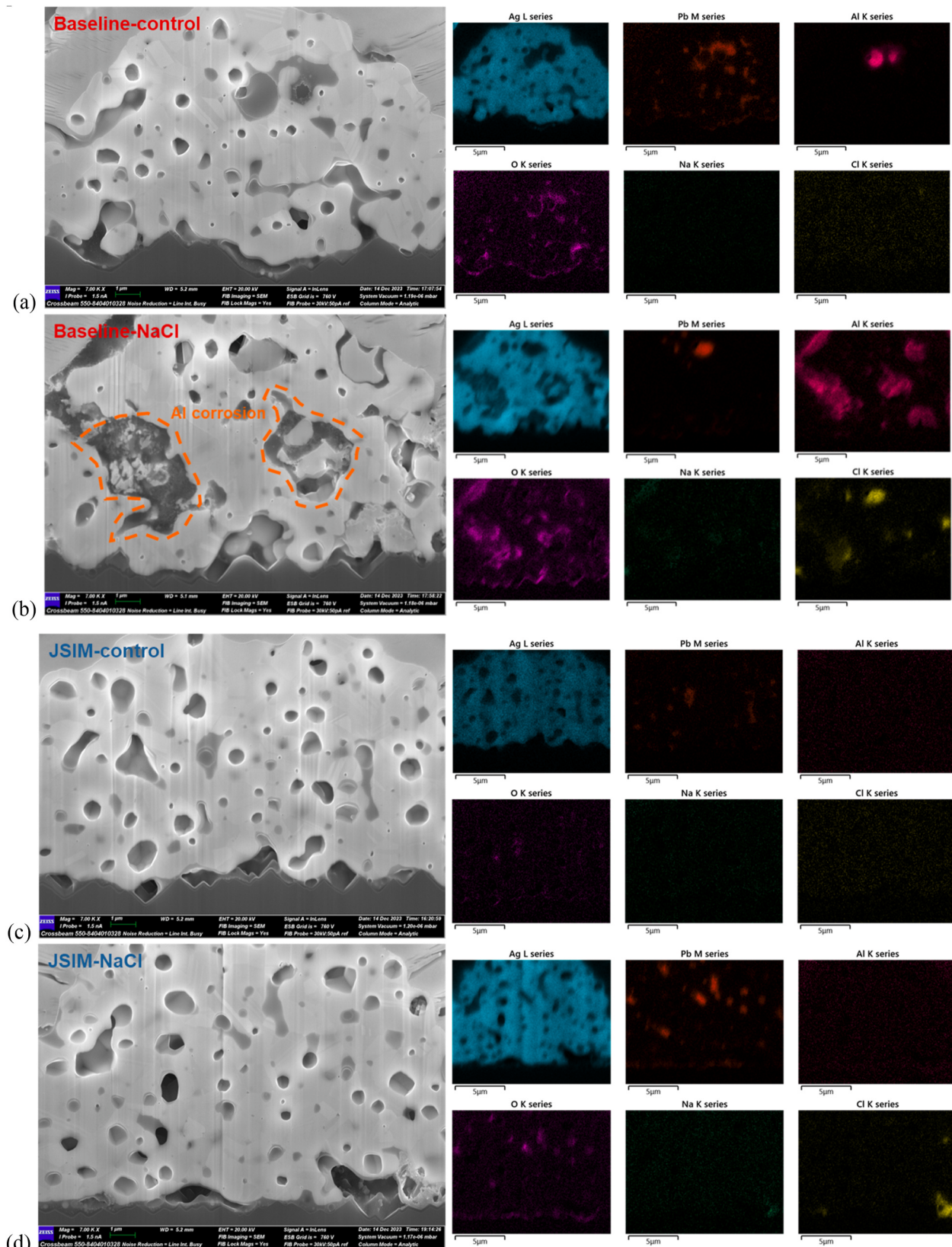


Fig. 7. Cross-section SEM images of front-side TOPCon samples after 40-h DH85 and corresponding EDS mappings of Ag, Pb, Al, O, Na, Cl. The samples were prepared by cryo-FIB and the description of the samples can be found in Fig. 1.

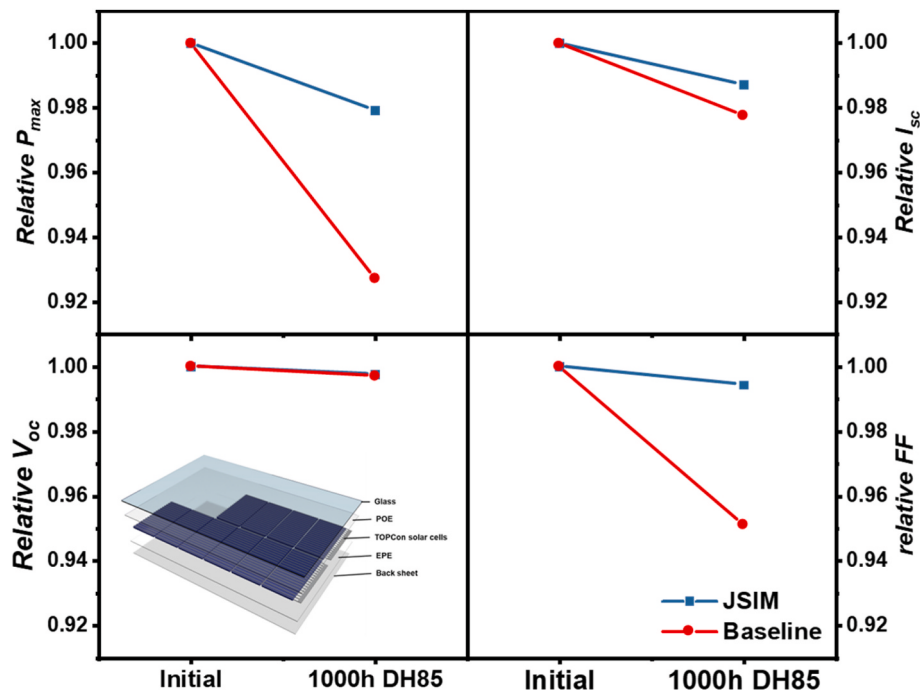


Fig. 8. Relative change in module I - V parameters for glass-backsheet (G-B) modules fabricated with JSIM and baseline TOPCon solar cells after 1000 hours of DH85.

only a trace amount of Cl at the Si/Ag interface, suggesting that NaCl induced some reaction on the Ag/Si alloy but was limited to exposed regions. No indications of metal or glass frit failures were evident within the contact. Unlike the baseline samples, NaCl did not induce any reaction within the JSIM metal contacts.

Consequently, JSIM TOPCon solar cells show an increased resistance to NaCl corrosion under DH85 conditions and experienced less PCE loss compared to baseline TOPCon solar cells during the testing period. Our results are consistent with the hypothesis that the Al content in the metallization paste is the main cause for its low corrosion resistance, and thus, reducing or removing Al from the paste results in TOPCon solar

cells with a high corrosion resistance.

3.5. Module results

To further substantiate the stability of JSIM TOPCon solar cells, we fabricated commercial-sized G-B modules comprising 144 half-cut cells and subjected them to standard module-level DH85 testing and compared the results to modules made using baseline solar cells. Throughout the testing phase, electroluminescence imaging was conducted to detect potential additional cracks or other module failures. The I - V results are shown in Fig. 8. Following 1000 h of DH85 testing,

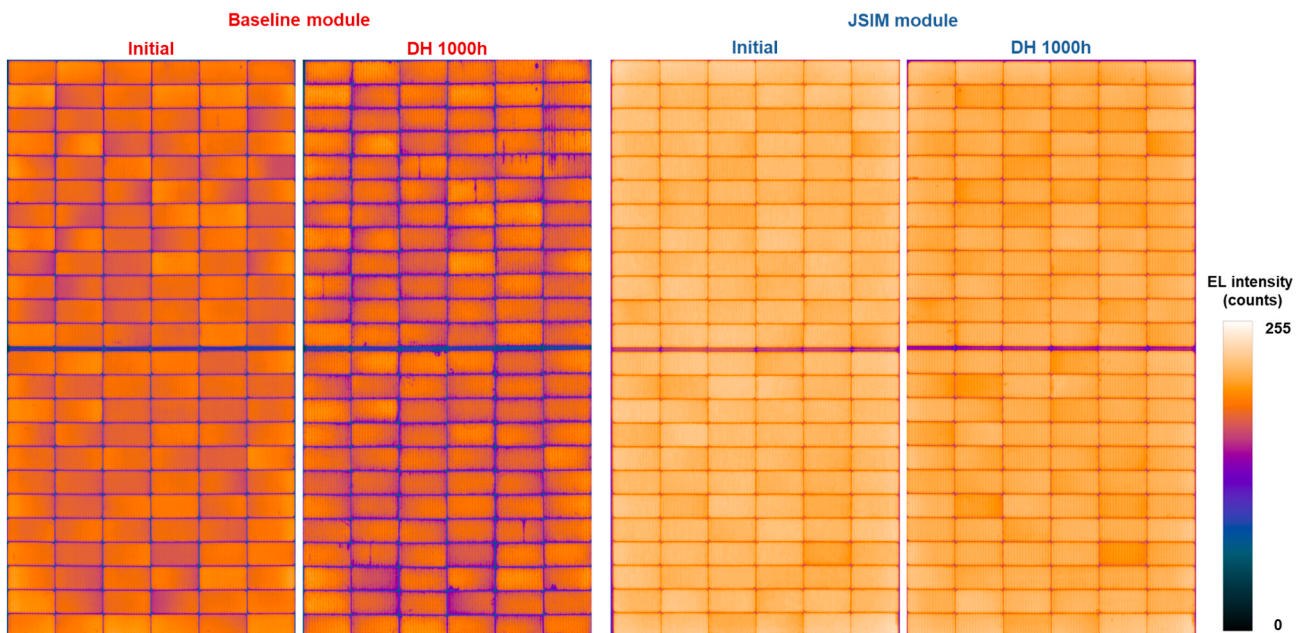


Fig. 9. Electroluminescence images of JSIM and baseline modules before and after 1000-h DH85 testing.

JSIM modules experienced only a $\sim 2.1\%$ _{rel} decrease in maximum power (P_{max}), whereas baseline modules encountered a more substantial $\sim 7.3\%$ _{rel} reduction in PCE. The reduction in short-circuit current (I_{sc}) was $\sim 1.2\%$ _{rel} for JSIM modules and $\sim 2.2\%$ _{rel} for baseline modules, while both exhibited a $\sim 0.2\%$ _{rel} loss in V_{oc} . The cause for the drop in I_{sc} is likely related to changes in the optics of the module which are not related to the solar cells and thus were omitted from the further discussion. The minimal loss in V_{oc} is consistent with the results presented in Sections 3.1 to 3.3, which indicated that corrosion predominantly affects the series resistance of the solar cells, i.e., affecting the FF of the module. The JSIM modules exhibited a $\sim 0.6\%$ _{rel} FF decline, whereas baseline modules suffered a significantly higher $\sim 4.9\%$ _{rel} FF loss. This is consistent with an increase of R_s at the module level due to cell-level contact degradation in baseline modules. Overall, JSIM G-B modules demonstrated superior reliability under DH85 conditions, showcasing better stability compared to their baseline counterparts.

The electroluminescence images of JSIM and baseline modules shown in Fig. 9 reveal no discernible differences between the JSIM modules. However, in baseline modules, noticeable failure patterns are evident along the contacts. This serves as additional evidence supporting the long-term stability of JSIM TOPCon cells within G-B modules.

4. Conclusion

TOPCon technology is expected to become the dominant technology in 2024 due to its higher efficiency and relatively low manufacturing costs. Unfortunately, various reports have shown that the TOPCon technology is more sensitive to degradation, in particular corrosion, and this could potentially result in higher yearly degradation negatively affecting the leveled costs of electricity (LCOE) of the TOPCon technology. This study demonstrates that laser-assisted firing significantly enhances the corrosion resistance of TOPCon solar cells. This improvement is attributed to the broader processing window offered by the firing technique and the capability to employ pastes that do not contain aluminum to contact the lightly-doped boron surface at the front of the TOPCon solar cell. In this work we used the Jolywood Special Injected Metallization (JSIM) method and compared it to baseline TOPCon solar cells fabricated using conventional pastes and firing. Solar cells were exposed to NaCl and underwent 20 h of damp heat testing under 85 °C and 85% relative humidity (DH85). The baseline cells demonstrated rapid degradation, while JSIM cells only showed a minor drop in performance. The contact resistance of the NaCl-exposed JSIM cells was relatively unaffected by after 20 h of DH85, while the NaCl-exposed solar cells contact resistance increased by over two orders of magnitude. Scanning electron microscopy confirm significant chemical reactions in the baseline solar cells, in particular related to Al, consistent with the hypothesis that the relatively high Al content, used to improve the electrical contact between the metal paste and the lightly boron-doped silicon surface, is the cause for its low corrosion-resistance. The cell results were confirmed at the module level where JSIM TOPCon G-B modules demonstrated superior reliability compared to baseline TOPCon modules after module DH85 testing. Consequently, this work shows that laser-assisted firing process such as JSIM can significantly improve the intrinsic corrosion-resistance of TOPCon solar cells. This not only results in more stable TOPCon modules, but also enables the use of lower cost bill of materials for the TOPCon technology, further reducing the LCOE of this technology.

CRediT authorship contribution statement

Xinyuan Wu: Writing – original draft, Visualization, Validation, Methodology, Investigation, Formal analysis, Data curation, Conceptualization. **Xutao Wang:** Investigation, Formal analysis, Data curation. **Weiguang Yang:** Writing – review & editing, Resources, Project administration, Investigation, Data curation. **Jianjun Nie:** Investigation, Data curation. **Jing Yuan:** Investigation, Formal analysis, Data

curation. **Muhammad Umair Khan:** Investigation. **Alison Ciesla:** Supervision, Methodology. **Chandany Sen:** Writing – review & editing, Supervision, Methodology, Investigation, Formal analysis, Data curation. **Zhencong Qiao:** Resources. **Bram Hoex:** Writing – review & editing, Visualization, Validation, Supervision, Resources, Project administration, Investigation, Funding acquisition, Conceptualization.

Declaration of competing interest

The authors declare the following financial interests/personal relationships which may be considered as potential competing interests.

Bram Hoex reports financial support was provided by Australian Renewable Energy Agency. Bram Hoex and Chandany Sen report a relationship with Australian Centre for Advanced Photovoltaics that includes: funding grants. If there are other authors, they declare that they have no known competing financial interests or personal relationships that could have appeared to influence the work reported in this paper.

Data availability

Data will be made available on request.

Acknowledgements

The work is partly supported by the Australian Centre for Advanced Photovoltaics(ACAP) and received funding from the Australian Renewable Energy Agency (ARENA). However, the Australian Government does not accept responsibility for the views, information, or advice expressed in this research. This work was also supported by the Special Fund for Carbon Peak Carbon Neutralization Technology Innovation Program grant funded by the Jiangsu Provincial Department of Science and Technology within the project “Research on Key Technologies and Industrialization of Efficient N-type Bifacial TOPCon Solar Cells” (Project No.:BA2022204). The authors would like to acknowledge the Electron Microscope Unit at The University of New South Wales (UNSW), specifically Dr Yin Yao and Dr Charlie Kong, for their scientific and technical assistance and access to the facilities of the Australian Microscopy & Microanalysis Research Facility. The authors also express their gratitude for the support provided by the Solar Industrial Research Facility (SIRF) at UNSW. Furthermore, Xinyuan Wu acknowledges the support received from the Australian Government Research Training Program (RTP) Scholarship.

References

- [1] F. Feldmann, M. Bivour, C. Reichel, M. Hermle, S.W. Glunz, A passivated rear contact for high-efficiency n-type silicon solar cells enabling high Voc and FF> 82%, in: 28th European PV Solar Energy Conference and Exhibition, 2013.
- [2] F. Feldmann, M. Simon, M. Bivour, C. Reichel, M. Hermle, S.W. Glunz, Carrier-selective contacts for Si solar cells, Appl. Phys. Lett. 104 (18) (2014) 181105, <https://doi.org/10.1063/1.4875904>, 2014-05-05.
- [3] F. Feldmann, M. Bivour, C. Reichel, M. Hermle, S.W. Glunz, Passivated rear contacts for high-efficiency n-type Si solar cells providing high interface passivation quality and excellent transport characteristics, Sol. Energy Mater. Sol. Cell. 120 (2014) 270–274.
- [4] A. Richter, J. Benick, F. Feldmann, A. Fell, M. Hermle, S.W. Glunz, n-Type Si solar cells with passivating electron contact: identifying sources for efficiency limitations by wafer thickness and resistivity variation, Sol. Energy Mater. Sol. Cell. 173 (2017) 96–105, <https://doi.org/10.1016/j.solmat.2017.05.042>, 2017-12-01.
- [5] A. Richter, et al., Design rules for high-efficiency both-sides-contacted silicon solar cells with balanced charge carrier transport and recombination losses, Nat. Energy 6 (4) (2021) 429–438, <https://doi.org/10.1038/s41560-021-00805-w>, 2021-04-01.
- [6] T. Gao, et al., An industrially viable TOPCon structure with both ultra-thin SiOx and n+-poly-Si processed by PECVD for p-type c-Si solar cells, Sol. Energy Mater. Sol. Cell. 200 (2019) 109926, <https://doi.org/10.1016/j.solmat.2019.109926>, 2019-09-01.
- [7] Z. Zhang, et al., Improvement of surface passivation of tunnel oxide passivated contact structure by thermal annealing in mixture of water vapor and nitrogen environment, Sol. RRL 3 (10) (2019) 1900105, <https://doi.org/10.1002/solr.201900105>, 2019-10-01.

- [8] X. Guo, et al., Comparison of different types of interfacial oxides on hole-selective p+-poly-Si passivated contacts for high-efficiency c-Si solar cells, *Sol. Energy Mater. Sol. Cell.* 210 (2020) 110487, <https://doi.org/10.1016/j.solmat.2020.110487>, 2020-06-01.
- [9] Y. Huang, et al., Ultrathin silicon oxide prepared by in-line plasma-assisted N₂O oxidation (PANO) and the application for n-type polysilicon passivated contact, *Sol. Energy Mater. Sol. Cell.* 208 (2020) 110389, <https://doi.org/10.1016/j.solmat.2019.110389>, 2020-05-01.
- [10] B. Liao, J. Ge, X. Wu, Q. Wang, R.J. Yeo, Z. Du, Unlocking the potential of borosilicate glass passivation for industrial tunnel oxide passivated contact solar cells, *Prog. Photovoltaics Res. Appl.* 30 (3) (2022) 310–317.
- [11] B. Liao, et al., Tube-type plasma-enhanced atomic layer deposition of aluminum oxide: enabling record lab performance for the industry with demonstrated cell efficiencies >24, *Prog. Photovoltaics Res. Appl.* 31 (1) (2023) 52–61, <https://doi.org/10.1002/pip.3607>, 2023-01-01.
- [12] B. Liao, et al., Atomic scale controlled tunnel oxide enabled by a novel industrial tube-based PEALD technology with demonstrated commercial TOPCon cell efficiencies > 24, *Prog. Photovoltaics Res. Appl.* 31 (3) (2023) 220–229, <https://doi.org/10.1002/pip.3627>, 2023-03-01.
- [13] M. Fischer, M. Woodhouse, P. Ballozian, J. Trube, International Technology Roadmap for Photovoltaic (ITRPV) 2022 Results, VDMA, 2023.
- [14] P.M. Sommeling, J. Liu, J.M. Kroon, Corrosion effects in bifacial crystalline silicon PV modules: interactions between metallization and encapsulation, *Sol. Energy Mater. Sol. Cell.* 256 (2023) 112321, <https://doi.org/10.1016/j.solmat.2023.112321>, 2023/07/01/.
- [15] N. Iqbal, et al., Impact of acetic acid exposure on metal contact degradation of different crystalline silicon solar cell technologies, *Sol. Energy Mater. Sol. Cell.* 250 (2023) 112089, <https://doi.org/10.1016/j.solmat.2022.112089>, 2023/01/15/.
- [16] M. Köntges, et al., Review of Failures of Photovoltaic Modules, 2014.
- [17] M. Aghaei, et al., Review of degradation and failure phenomena in photovoltaic modules, *Renew. Sustain. Energy Rev.* 159 (2022) 112160, <https://doi.org/10.1016/j.rser.2022.112160>, 2022/05/01/.
- [18] W. Oh, et al., The degradation of multi-crystalline silicon solar cells after damp heat tests, *Microelectron. Reliab.* 54 (9) (2014) 2176–2179, <https://doi.org/10.1016/j.microrel.2014.07.071>, 2014/09/01/.
- [19] A. Ndiaye, C.M.F. Kébé, A. Charki, P.A. Ndiaye, V. Sambou, A. Kobi, Degradation evaluation of crystalline-silicon photovoltaic modules after a few operation years in a tropical environment, *Sol. Energy* 103 (2014) 70–77, <https://doi.org/10.1016/j.solener.2014.02.006>, 2014/05/01/.
- [20] Y. Zhou, D. Chen, Y. Ye, H. Yin, X. Niu, Damp-Heat Endurance Investigation of PV Modules Based on N-type Bifacial Passivated Contact Cells, EU PVSEC 2023, 2023.
- [21] C. Sen, et al., Accelerated damp-heat testing at the cell-level of bifacial silicon HJT, PERC and TOPCon solar cells using sodium chloride, *Sol. Energy Mater. Sol. Cell.* 262 (2023) 112554, <https://doi.org/10.1016/j.solmat.2023.112554>, 2023/10/15/.
- [22] C. Peike, et al., Origin of damp-heat induced cell degradation, *Sol. Energy Mater. Sol. Cell.* 116 (2013) 49–54, <https://doi.org/10.1016/j.solmat.2013.03.022>, 2013/09/01/.
- [23] M. Koehl, S. Hoffmann, S. Wiesmeier, Evaluation of damp-heat testing of photovoltaic modules, *Prog. Photovoltaics Res. Appl.* 25 (2) (2017) 175–183, <https://doi.org/10.1002/pip.2842>, 2017-02-01.
- [24] P. Afzali, M. Yousefpour, E. Borhani, Evaluation of the effect of ageing heat treatment on corrosion resistance of Al-Ag alloy using electrochemical methods, *J. Mater. Res.* 31 (16) (2016) 2457–2464.
- [25] P. Afzali, M. Yousefpour, E. Borhani, Effect of deformation-induced defects on the microstructure and pitting corrosion behavior of Al-Ag alloy, *Int. J. Eng.* 31 (12) (2018) 2092–2101.
- [26] S.-W. Fu, C.C. Lee, A corrosion study of Ag-Al intermetallic compounds in chlorine-containing epoxy molding compounds, *J. Mater. Sci. Mater. Electron.* 28 (20) (2017) 15739–15747, <https://doi.org/10.1007/s10854-017-7467-4>, 2017-10-01.
- [27] T. Semba, New corrosion mechanism observed at Ag/Al metallization of n-type bifacial solar cells, in: 2020 47th IEEE Photovoltaic Specialists Conference (PVSC), IEEE, 2020, pp. 850–853.
- [28] E. Schneiderlöchner, R. Preu, R. Lüdemann, S.W. Glunz, Laser-fired rear contacts for crystalline silicon solar cells, *Prog. Photovoltaics Res. Appl.* 10 (1) (2002) 29–34, <https://doi.org/10.1002/pip.422>, 2002-01-01.
- [29] M. Weizman, et al., Efficiency and stability enhancement of laser-crystallized polycrystalline silicon thin-film solar cells by laser firing of the absorber contacts, *Sol. Energy Mater. Sol. Cell.* 120 (2014) 521–525, <https://doi.org/10.1016/j.solmat.2013.09.033>, 2014/01/01/.
- [30] P. Ortega, et al., Laser-fired contact optimization in c-Si solar cells, *Prog. Photovoltaics Res. Appl.* 20 (2) (2012) 173–180, <https://doi.org/10.1002/pip.1115>, 2012-03-01.
- [31] I. Sanchez-Aniora, et al., Optimization of laser-firing processes for silicon-heterojunction solar-cell back contacts, *Appl. Surf. Sci.* 258 (23) (2012) 9443–9446.
- [32] S. Glunz, et al., Laser-fired contact silicon solar cells on p-and n-substrates, in: 19th European Photovoltaic Solar Energy Conference, 2004, p. 11.
- [33] D. Ourinson, et al., Laser-powered Co-firing process for highly efficient Si solar cells, *IEEE J. Photovoltaics* 11 (2) (2021) 282–288.
- [34] R. Mayberry, K. Myers, V. Chandrasekaran, A. Henning, H. Zhao, u.E. Hofmüller, Laser enhanced contact optimization (LECO) and LECO-Specific pastes—A novel technology for improved cell efficiency, in: 36th European Photovoltaic Solar Energy Conference and Exhibition, 2019.
- [35] H. Höffler, T. Fellmeth, F. Maischner, J. Greulich, E. Krassowski, A. Henning, Enlarged firing window and efficiency boosting of PERC solar cells by 'laser enhanced contact optimization'(LECO), *AIP Conf. Proc.* 2487 (1) (2022). AIP Publishing.
- [36] E. Krassowski, S. Großer, M. Turek, A. Henning, H. Zhao, Investigation of monocrystalline p-type PERC cells featuring the laser enhanced contact optimization process and new LECO paste, *AIP Conf. Proc.* 2367 (1) (2021). AIP Publishing.
- [37] T. Fellmeth, et al., Laser-enhanced contact optimization on iTOPCon solar cells, *Prog. Photovoltaics Res. Appl.* 30 (12) (2022) 1393–1399.
- [38] E. Krassowski, et al., Reliability evaluation of photovoltaic modules fabricated from treated solar cells by laser-enhanced contact optimization process, *Sol. RRL* 6 (5) (2022) 2100537.
- [39] E. Krassowski, T. Luka, V. Naumann, M. Turek, S. Großer, H. Zhao, Degradation stability of solar cells after laser enhanced contact optimization (LECO), *AIP Conf. Proc.* 2487 (1) (2022). AIP Publishing.
- [40] IEC TS 62782, 2016 Photovoltaic (PV) Modules - Cyclic (Dynamic) Mechanical Load Testing, I. E. Commission, 2016, 2016-03-09, <https://webstore.iec.ch/publication/24310>.
- [41] D.N.R. Payne, C. Vargas, Z. Hameiri, S.R. Wernham, D.M. Bagnall, An advanced software suite for the processing and analysis of silicon luminescence images, *Comput. Phys. Commun.* 215 (2017) 223–234, <https://doi.org/10.1016/j.cpc.2017.02.012>, 2017/06/01/.
- [42] A.V. Benedetti, P.T.A. Sumodjo, K. Nobe, P.L. Cabot, W.G. Proud, Electrochemical studies of copper, copper-aluminium and copper-aluminium-silver alloys: impedance results in 0.5M NaCl, *Electrochim. Acta* 40 (16) (1995) 2657–2668, [https://doi.org/10.1016/0013-4686\(95\)00108-Q](https://doi.org/10.1016/0013-4686(95)00108-Q), 1995/11/01/.
- [43] Q. Zhang, Z. Zhang, On the electrochemical dealloying of Al-based alloys in a NaCl aqueous solution, *Phys. Chem. Chem. Phys.* 12 (7) (2010) 1453–1472, <https://doi.org/10.1039/b919313h>, 2010-01-01.
- [44] M. Trueba, S.P. Trasatti, Study of Al alloy corrosion in neutral NaCl by the pitting scan technique, *Mater. Chem. Phys.* 121 (3) (2010) 523–533.
- [45] M. Jingling, W. Jiuba, L. Gengxin, X. Chunhua, The corrosion behaviour of Al-Zn-In-Mg-Ti alloy in NaCl solution, *Corrosion Sci.* 52 (2) (2010) 534–539.
- [46] Y. Hao, H. Yang, H. Han, C. Nan, X. Huang, H. Wang, Potential-induced electrochemical corrosion in crystalline silicon solar cells, *Sol. RRL* (2024) 2300980.
- [47] S. Tepner, A. Lorenz, Printing technologies for silicon solar cell metallization: a comprehensive review, *Prog. Photovoltaics Res. Appl.* 31 (6) (2023) 557–590.
- [48] Y.-W. Ok, J.-H. Kim, V.D. Upadhyaya, A. Rohatgi, C.-H. Hong, C.-J. Choi, Dose-dependency of contact resistance and sheet resistance of B-implanted emitters for N-type crystalline Si solar cells fabricated using screen-printed fire-through Ag/Al paste metallization process, *J. Kor. Phys. Soc.* 82 (7) (2023) 707–711.